ASM Handbook, Volume 10, *Materials Characterization*
ASM Handbook Committee
DOI 10.31399/asm.hb.v10.a0006685

Raman Spectroscopy*

Overview

General Uses

- Molecular analysis of bulk samples and surface or near-surface species as identified by their characteristic vibrational frequencies
- Low-frequency vibrational information on solids for metal-ligand vibrations and lattice vibrations
- Determination of phase composition of solids

Examples of Applications

- Identification of effects of preparation on glass structure
- Structural analysis of polymers
- Determination of structural disorder in graphites
- Determination of surface structure of metal oxide catalysts
- Identification of corrosion products on metals
- Identification of surface adsorbates on metal electrodes

Samples

- *Form:* Solid, liquid, or gas
- *Size:* Single crystal of material to virtually any size the Raman spectrometer can accommodate

Limitations

- *Sensitivity:* Poor to fair without enhancement
- Raman spectroscopy requires concentrations greater than approximately 1 to 5%
- Analysis of surface or near-surface species difficult but possible
- Sample fluorescence or impurity fluorescence may prohibit Raman characterization

Estimated Analysis Time

- 30 min to 8 h per sample

Capabilities of Related Techniques

- *Infrared spectroscopy and Fourier-transform infrared spectroscopy:* Molecular vibrational identification of materials; lacks sensitivity to surface species; difficult on aqueous systems
- *High-resolution electron energy loss spectroscopy:* Vibrational analysis of surface species in ultrahigh-vacuum environment; extremely sensitive; requires ultrahigh-vacuum setup; low resolution compared to Raman spectroscopy; cannot be used for *in situ* studies

Introduction

Raman spectroscopy is a valuable tool for the characterization of materials due to its extreme sensitivity to the molecular environment of the species of interest. Information on molecular vibrations can provide much structural, orientational, and chemical information that can assist in defining the environment of the molecule of interest to a high degree of specificity. The materials applications for which Raman spectroscopy can be used continue to expand with improvements in requisite instrumentation and methodology.

This article will introduce principles of Raman spectroscopy and the representative materials characterization applications to which Raman spectroscopy has been applied. The section "The Raman Effect" includes a discussion of light-scattering fundamentals and a description of the experimental aspects of the technique. Emphasis has been placed on the different instrument approaches that have been developed for performing Raman analyses on various materials. The applications presented reflect the breadth of materials characterization uses for Raman spectroscopy and highlight the analysis of bulk material and of surface and near-surface species.

The Raman Effect

Fundamentals

Raman spectroscopy is one of many light-scattering phenomena. All these phenomena originate from the principle that the intensity of a beam of light decreases measurably when it passes through a nonabsorbing medium. The energy lost is not significantly degraded to heat. Rather, some of the light energy is scattered into the space surrounding the sample.

The Raman effect is named after C.V. Raman, who, with K.S. Krishnan, first observed this phenomenon in 1928 (Ref 1). It belongs to the class of molecular-scattering phenomena. The molecular-scattering phenomena that must be considered are Rayleigh scattering, Stokes scattering (the normal Raman effect), and anti-Stokes scattering. The nature of this scattered radiation is predicted by quantum theory and classical electromagnetic theory.

The quantum theory of Raman scattering involves consideration of radiation of frequency v_0 as consisting of photons that have energy hv_0. Scattering of this radiation occurs

*Reprinted from J.E. Pemberton and A.L. Guy, Raman Spectroscopy, *Materials Characterization*, Vol 10, *ASM Handbook*, ASM International, 1986, p 126–138

when these photons undergo two types of collisions with the molecules of a medium. These collisions are shown as energy-level diagrams in Fig. 1. Elastic collisions are those in which the energy of the scattered photon, $h\nu_s$, is unchanged relative to the initial energy of the incident photon; that is, $h\nu_s = h\nu_0$. This is known as Rayleigh scattering and is the most probable scattering that will occur in a molecular system.

Much less probable is the inelastic collision of a photon with a molecule. In this case, energy is exchanged between the photon and the molecule such that the scattered photon is of higher or lower energy than the incident photon. The energy of the scattered photons in these types of scattering events is $h(\nu_0 \pm \nu_n)$. Because the energy levels of the molecule are discrete and well defined, energy can be lost or gained by the molecule only in quantized or discrete amounts. Therefore, two types of scattered radiation result from these inelastic scattering events.

Stokes radiation, the first type, is observed for molecules that gain a vibrational or rotational quantum of energy from the incident photon. When this occurs, the scattered photon is lower in energy than the incident photon by an amount $h\nu_n$ that equals the amount of energy required to excite a vibration or rotation in the molecule. The energy of the Stokes-scattered photon, $h\nu_S$, is $h(\nu_0 - \nu_n)$. Anti-Stokes radiation, the second type, is observed for molecules that lose a vibrational or rotational quantum of energy to the incident photon. The energy of the anti-Stokes scattered photon, $h\nu_{AS}$, is $h(\nu_0 + \nu_n)$. All these scattering events occur within 10^{-12} to 10^{-13} s.

Because anti-Stokes scattering can occur only for molecules that are in an excited vibrational or rotational state before scattering, the intensity of anti-Stokes radiation is significantly less than that of Stokes radiation at room temperature. Therefore, Raman spectroscopy generally uses Stokes radiation. Overall, however, the total amount of inelastically scattered Stokes and anti-Stokes radiation is small compared to the elastically scattered Rayleigh radiation. This feature of molecular scattering makes the detection of Stokes radiation a serious problem.

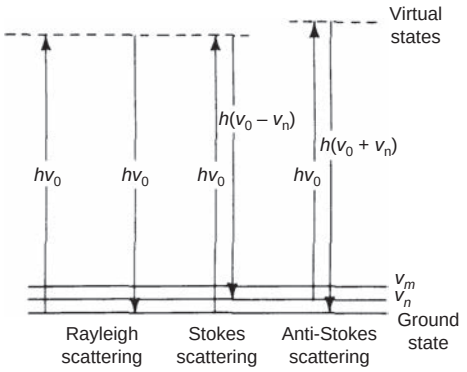

Fig. 1 Energy-level diagram of molecular light-scattering processes.

When a molecule is in an electromagnetic field, it is distorted by the attraction of the electrons to the positive pole of the electric field and the attraction of the nuclei to the negative pole of the electric field. The extent to which this distortion occurs is a characteristic of the molecule known as its polarizability. The resulting separation of charge produces a momentary induced electric dipole moment that is usually expressed as the dipole moment per unit volume and is known as the polarization, P. Under these circumstances the molecule is considered to be polarized.

The magnitude of polarization of a molecule depends on the magnitude of the electric field, E, and on the characteristics of the molecule describing the ease with which the molecule can be distorted, its polarizability (α). Therefore:

$$P = \alpha E \qquad \text{(Eq 1)}$$

The oscillating electric field in an electromagnetic wave is:

$$E = E_0 \cos(2\pi\nu_0) \qquad \text{(Eq 2)}$$

The induced dipole also oscillates at frequency ν_0. Therefore:

$$P = \alpha E_0 \cos(2\pi\nu_0 t) \qquad \text{(Eq 3)}$$

According to classical electromagnetic theory, such an oscillating dipole moment can act as a source of radiation. Rayleigh scattering arises from radiation that the oscillating dipole emits at its own frequency, ν_0. If the molecule also undergoes some internal motion, such as vibration or rotation, that periodically changes the polarizability, the oscillating dipole will have superimposed on it the vibrational or rotational frequency. This effect is mathematically based on the equation describing the polarizability of the molecule. Polarizability, α, is:

$$\alpha = \alpha_0 + \sum_n \alpha_n \cos(2\pi\nu_n t) \qquad \text{(Eq 4)}$$

where α_0 is the static polarizability of the molecule, which in part produces Rayleigh scattering. The second term in the polarizability expression is a sum of terms having the periodic time dependence of the normal frequencies of the internal motions of the molecule. Substituting this expression for the polarizability into Eq 3 yields:

$$P = E_0\alpha_0 \cos(2\pi\nu_0 t) + E_0 \sum_n \alpha_n \cos(2\pi\nu_0 t) \cos(2\pi\nu_n t) \qquad \text{(Eq 5)}$$

This can be expanded to provide:

$$P = E_0\alpha_0 \cos(2\pi\nu_0 t) + \tfrac{1}{2}E_0 \sum_n \alpha_n [\cos 2\pi(\nu_0 - \nu_n)t + \cos 2\pi(\nu_0 + \nu_n)t] \qquad \text{(Eq 6)}$$

This equation predicts three components of the scattered radiation. The first term predicts scattering of radiation at the incident frequency, ν_0, or Rayleigh scattering. The second term predicts scattering at frequencies lower than the incident frequency by amounts corresponding to the normal frequencies of the molecule, $(\nu_0 - \nu_n)$. This is Stokes scattering. The third term predicts scattering at frequencies higher than that of the incident frequency by amounts corresponding to the normal frequencies of the molecule, $(\nu_0 + \nu_n)$. This is anti-Stokes scattering.

Polarizability is a tensor that leads to important consequences in the angular dependence and polarization of the scattered radiation. Therefore, the relationship between polarization and the electric field vector is more accurately written in matrix notation:

$$\begin{vmatrix} P_x \\ P_y \\ P_z \end{vmatrix} = \begin{vmatrix} \alpha_{xx} & \alpha_{xy} & \alpha_{xz} \\ \alpha_{yx} & \alpha_{yy} & \alpha_{yz} \\ \alpha_{zx} & \alpha_{zy} & \alpha_{zz} \end{vmatrix} \begin{vmatrix} E_x \\ E_y \\ E_z \end{vmatrix} \qquad \text{(Eq 7)}$$

This relationship also has consequences regarding selection rules in Raman spectroscopy. If a vibrational mode is to be Raman active, the vibration must alter the polarizability of the molecule; that is, α_n must not equal zero. This selection rule is best put into context by contrasting it with the selection rule of another vibrational spectroscopy, infrared spectroscopy (the article "Infrared Spectroscopy" in this Volume supplies additional information on this technique). Infrared active modes of a molecule produce a change in true electric dipole moment existing in the molecule. This fundamental difference between these two vibrational spectroscopies leads to the complementary and sometimes mutually exclusive nature of the vibrational modes measured by infrared and Raman spectroscopies.

In terms of the experimental utility of Raman spectroscopy, the Raman intensity of a particular vibrational mode is proportional to the intensity of the incident radiation and proportional to the fourth power of the scattered-light frequency:

$$I_n = \frac{2^3}{3^3 c^4} I_0 (\nu_0 - \nu_n)^4_{i,j} (\alpha_{ij})^2_n \qquad \text{(Eq 8)}$$

This relationship indicates that the sensitivity of a Raman analysis can be improved by using higher excitation powers or by increasing the energy (frequency) of the excitation. Additional information on Raman intensities is cited in Ref 2 and 3.

Experimental Considerations

The inherent weakness of Raman scattering that produces the poor sensitivity of the technique precluded the widespread use of Raman spectroscopy for materials characterization until recently. The advent of the laser as an

intense, monochromatic light source revived interest in use of the Raman effect for the acquisition of molecularly specific information about materials.

Two types of Raman spectrometers are commonly used to analyze materials. A conventional scanning monochromator system is shown in Fig. 2. Figure 3 illustrates a Raman system developed around one of several multichannel detectors. The difference between these Raman spectrometers is the method of obtaining Raman intensity as a function of frequency information.

Lasers are used almost exclusively as excitation sources in Raman spectroscopy. Laser radiation, possessing intensity, monochromaticity, and collimation, is well suited as a Raman excitation source. The most commonly used lasers for Raman spectroscopy are continuous-wave gas lasers. The most prevalent of these include the argon, krypton, and helium-neon lasers. Broadband tunable dye lasers are also commonly used to extend excitation capabilities further into the red region of the spectrum. Information on the fundamentals of lasers is cited in Ref 4.

Typical laser powers used in Raman analyses range from several milliwatts to several watts. The laser beam is usually focused on the sample using a series of mirrors and lenses. Focusing of the beam results in luminous power densities of several watts to thousands of watts per square centimeter. For absorbing samples, these power densities can cause significant heating. One means of reducing the extent of heating is to focus the laser beam to a line on the sample using a cylindrical lens. This approach also produces scattered radiation in a lineshape such that the entrance slit of the monochromator can be completely filled with the slit-shaped image.

The output of either type of Raman system is a plot of scattered-light intensity as a function of frequency shift in which the shift is calculated relative to the laser line frequency that is assigned as zero. Presentation of the spectra in this way facilitates comparison with infrared spectra, because both spectra are on equivalent frequency scales.

Raman spectra can be plotted on a recording device in real time in the above-mentioned fashion. However, conventional recording devices are being replaced by microcomputer-based data systems that provide for data storage and subsequent manipulation. A data system is required when using multichannel detection systems.

The heart of any Raman system is the monochromator-detector assembly. Conventional scanning monochromators are usually based on the use of two dispersion stages (a double monochromator) or three dispersion stages (a triple monochromator). Multiple dispersion stages are essential in obtaining Raman spectra to reduce the amount of stray radiation reaching the detector. Figure 4 shows a plot of the intensity ratio of the grating scatter to the

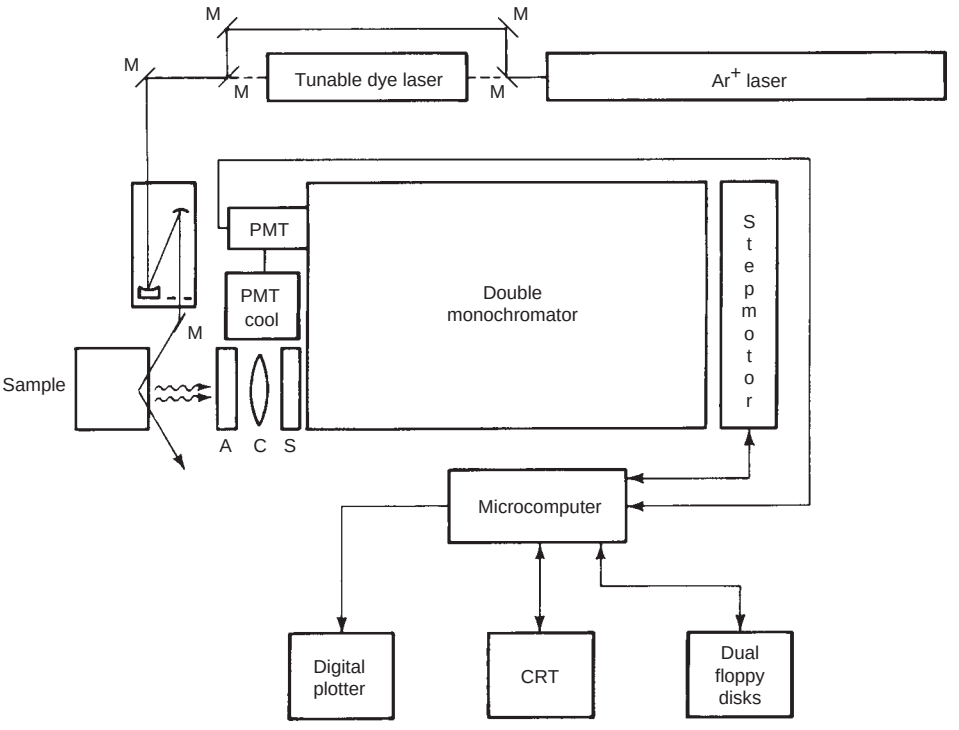

Fig. 2 Conventional Raman spectrometer. M, mirror; A, polarization analyzer; C, collection optics; S, polarization scrambler

Rayleigh scattering as a function of the Raman shift. This plot demonstrates that without multiple dispersion stages, the intensity of stray radiation can overshadow the much less intense Stokes-scattered radiation. In these devices, the dispersion elements are ruled gratings. Commercial scanning systems generally incorporate gratings that are ruled holographically to reduce the effects of optical artifacts in the observed spectra.

Raman spectra are acquired using scanning monochromators by mechanical movement of the dispersion elements such that the single-element detector sequentially detects the frequencies of interest. High-sensitivity photomultiplier tubes (PMTs) cooled to −20 to −40 °C (−4 to −40 °F) to reduce the dark current are typically used.

An alternative for the acquisition of Raman spectra is use of multichannel detectors in conjunction with a dispersion stage. Vidicon and diode array detectors may be used. To meet the requirements of Raman spectroscopy, these detectors usually incorporate image intensifiers that increase sensitivity. The benefit of the multichannel detector is known as Fellgett's advantage or the multiplex advantage. This signal-to-noise ratio advantage or time advantage relative to the performance of a single-channel detector is realized, because many frequencies are detected simultaneously. Relative to a single-channel detector, a multichannel detector can increase the signal-to-noise ratio proportional to the square root of the number of individual spectral resolution

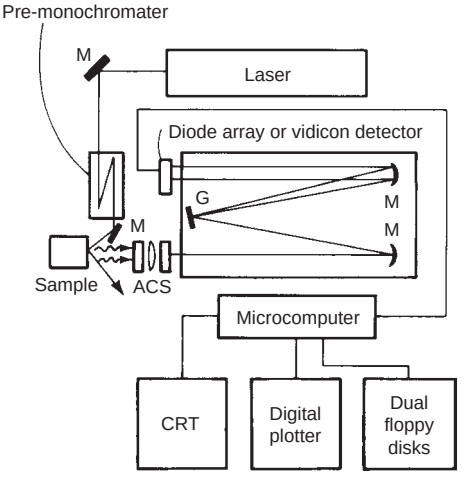

Fig. 3 Raman spectrometer with multichannel detector. M, mirror; G, grating; A, polarization analyzer; C, collection optics; S, polarization scrambler

elements simultaneously monitored by the multichannel detector.

Alternatively, Fellgett's advantage can be viewed as a time-saving benefit proportional to the square root of the number of spectral resolution elements. This is because a signal-to-noise ratio equivalent to that measured with a single-channel detector can be obtained in less time using a multichannel detector, assuming such factors as sensitivity and resolution equal those of a single-channel detector.

A single dispersion stage is the minimum requirement for use of a multichannel detector. Therefore, these detectors can be used with a single monochromator in many applications. However, problems can arise when using a single monochromator for Raman spectroscopy due to the poor stray light rejection capabilities of such a device. This problem has been addressed by the commercial availability of the Triplemate (Ref 5). This device incorporates a modified Czerny-Turner, zero-dispersion double spectrometer with a modified Czerny-Turner spectrograph. The double spectrometer acts as a wavelength-selectable interference filter, because the gratings disperse the radiation in opposite directions. Radiation is further dispersed in the final stage, and output at the exit is a line the width of the photosensitive area of the multichannel detector.

Multichannel systems may be used for investigation of kinetic phenomena and for Raman analysis of thermally labile species that would be decomposed by the laser beam in the time required to obtain the spectrum with a conventional system. Therefore, they may be useful in various materials characterization applications.

Sampling

Virtually any solid, liquid, or gas sample can be arranged to allow for acquisition of its Raman spectrum. Raman spectra of solid samples can be acquired in several ways. The solids can be in the form of pure powders in a glass capillary cell. Pure solids can be pressed into pellets or can first be mixed with an inert solid, such as potassium bromide (KBr), then pressed into pellets for characterization. Single crystals of organic or inorganic materials can be mounted on a goniometer head for Raman analysis. The presence of a fixed reference direction inside the crystal necessitates careful attention to the exact orientation of the direction of incidence of the exciting radiation and the direction of observation of the scattered radiation. Birefringence can be a problem in certain single crystals, depending on the symmetry of the species. Additional information on the optical properties of birefringent materials is cited in Ref 6.

A more recent development in the analysis of solid samples is the laser Raman molecular microprobe. This system is also termed the molecular optical laser examiner (MOLE) (Ref 7, 8). This innovative approach to the Raman characterization of materials allows molecular spectra to be obtained from samples on the microscopic level. Using this technique, the molecular components of a sample can be determined through their characteristic vibrational frequencies, and their distribution mapped across the sample. The instrument layout required for this technique is shown in Fig. 5.

The system is based on the single-channel detector/double monochromator arrangement or the multichannel detector/monochromator arrangement described above. A conventional optical microscope with bright- and dark-field illumination is the imaging system. The sample is placed on the microscope stage and can be analyzed in air, liquid, or a transparent medium. Two detectors are used in the system. The first is the PMT or multichannel detector for the acquisition of the actual spectra. The second is a TV detector that permits observation of the microstructure.

The MOLE can be operated in the punctual illumination or global illumination mode (Fig. 6). Punctual illumination allows recording of the Raman spectrum of one spot on the surface of the sample. This is also known as the spectral mode. Global illumination allows for obtaining the distribution or map of one component across the sample. Operation in this manner is also known as the imaging mode. The primary advantage of the laser Raman microprobe (MOLE) is that it provides molecular information on the microscale in a nondestructive analysis.

Raman spectroscopy may be used to analyze surface species, but its lack of sensitivity complicates these types of analyses. Several approaches are available to overcome the constraints imposed by the inherent weakness of the technique.

Raman spectra of surface species on high-surface-area solids, such as powders, are acquired easily in a glass capillary tube. Alternatively, powders can be pressed into pellets and analyzed. Careful analysis of species on metal surfaces also provides useful information. Raman analyses of these samples are usually performed by reflecting the laser beam off the metal surface and collecting the scattered radiation in the specular direction. Several mechanisms that enhance the intensity of the Raman-scattered radiation at metal surfaces under certain conditions may be used.

Several problems can arise in the Raman analysis of solids or surface species. Many solids frequently exhibit weak fluorescence, due to their inherent fluorescence or the presence of small amounts of fluorescent surface impurities. This fluorescence, even if weak,

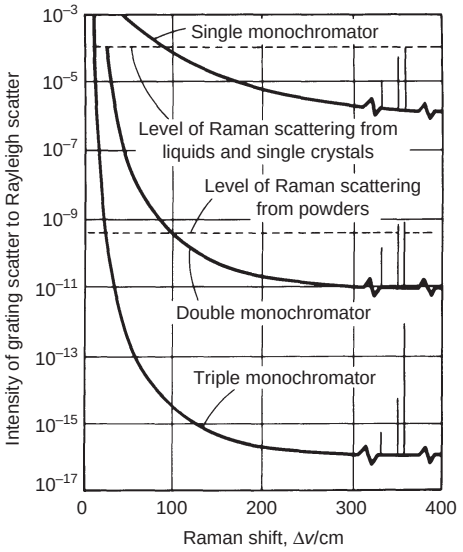

Fig. 4 Stray light rejection for single, double, and triple monochromators. Source: Ref 5

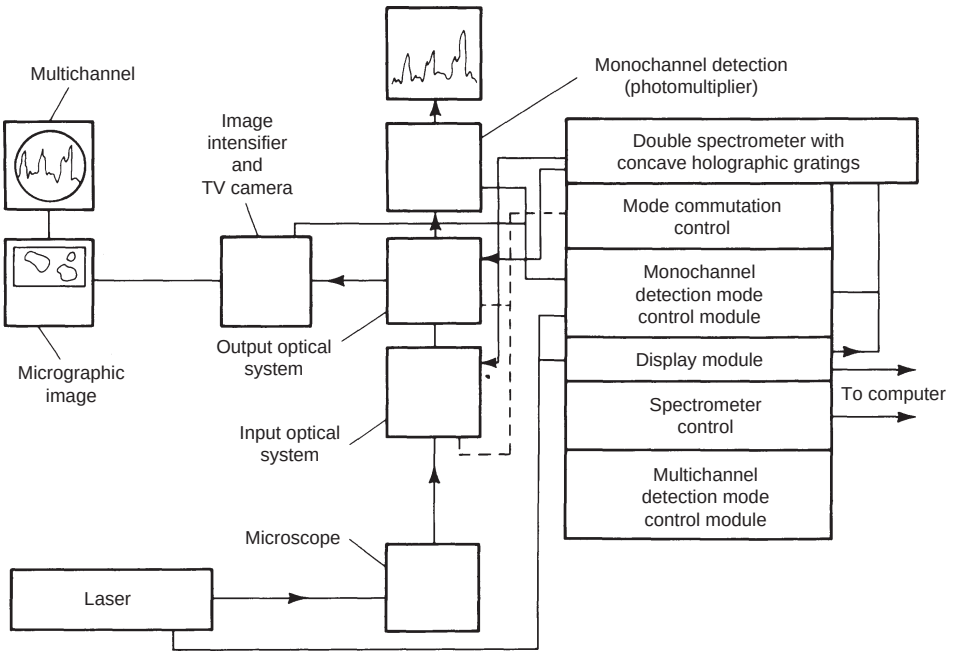

Fig. 5 Laser Raman microprobe. Source: Ref 8

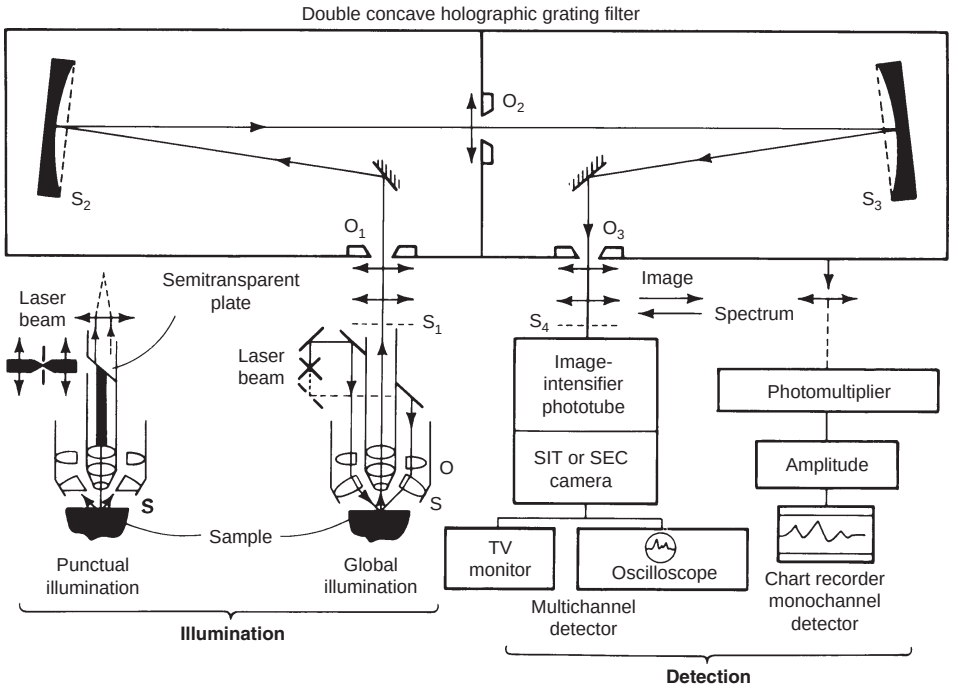

Fig. 6 Optical scheme of MOLE instrument. Source: Ref 8

will be more intense than the scattered radiation and will have noise associated with it. The Raman bands, which are superimposed on the fluorescence background, are often difficult to locate in the noise associated with fluorescence. The background fluorescence for silicas is fairly weak, but that for the alumina and silica-aluminas is considerably more intense (Ref 9). Various fluorescent impurities on solid surfaces have been identified. Hydrocarbons are commonly found on metal oxide surfaces (Ref 10-12). Trace amounts of transition metals have also been identified as sources of background fluorescence on aluminas and zeolites (Ref 13).

Few options are available in the analysis of inherently fluorescent solids. Extensive signal averaging to minimize the effect of the fluorescence noise may allow obtainment of partial Raman spectra. Significantly lowering the excitation energy may reduce the overall intensity of the fluorescence.

Removal of fluorescing impurities from the surface of solids to be analyzed requires treatment of these solids under rigorously controlled conditions. The most common surface impurities encountered are hydrocarbons (Ref 10-12). These can usually be removed by holding the sample several hours at elevated temperature in an oxygen or air atmosphere. Once cleaned, extreme care must be taken to avoid recontamination of sample surfaces through exposure to the ambient environment. Another approach to eliminating or reducing background fluorescence from impurities is preactivation of the sample by exposure to the laser beam for several hours before acquisition of the Raman spectrum (Ref 9).

A second problem frequently encountered in the Raman characterization of solids and surfaces is decomposition of the sample in the laser beam. One method of minimizing or eliminating this problem is to alter the laser conditions under which the sample is analyzed. Decreasing the laser power or changing the excitation frequency to a more suitable energy can help to eliminate the decomposition problem. A second approach is to rotate the sample such that the laser beam does not remain on any one spot on the sample long enough to cause extensive local heating and decomposition.

Sample decomposition is further exacerbated when analyzing samples that are highly absorbing at the excitation frequency used. The most effective method for handling highly absorbing samples is sample rotation (Ref 14). This approach has been frequently used for absorbing solids, such as graphites.

Information Obtainable from Raman Analyses

The type of molecular vibrations that produce Raman scattering must alter the polarizability of the molecule. Therefore, those vibrations that originate in relatively nonpolar bonds with symmetrical charge distributions produce the greatest polarizability changes and thus yield the most intense Raman scattering. Organic functional groups that fit these criteria include such moieties as C=C, C≡C, C≡N, C–N, N=N, C–S, S–S, and S–H.

However, functional group information is not the only type of vibrational information present in a Raman spectrum. Raman spectra of solids and crystals also contain contributions from lattice vibrations at low frequencies. These vibrations are due to the vibration of the molecules around their centers of mass or the restricted translation of molecules relative to each other. Lattice vibrations can provide a wealth of information on crystal forces (Ref 2).

Analysis of Bulk Materials

Metal Oxide Systems

Raman spectroscopy has been used with considerable success in the analysis of metal oxide systems. Metal oxide glasses provide particularly illustrative examples. Raman spectroscopy was initially applied to the investigation of glasses to overcome the problems of infrared analysis of these materials. Metal oxides exhibit strong absorption in the infrared region, making analysis of bulk metal oxides virtually impossible. Therefore, alkali halide pellets, for example, KBr, of the metal oxides usually must be prepared.

One possible consequence of this type of preparation—ion exchange of the metal oxide with the alkali halide—is a serious limitation to the infrared analysis of these materials. The chemical interaction between the metal oxide and the matrix changes the composition of the metal oxide under investigation. However, Raman scattering from metal oxides is usually only of weak to medium intensity. Therefore, bulk metal oxides can be analyzed easily without the chemical complications of infrared analysis.

An early Raman study of the influence of various cations on the bonding in the phosphate skeleton in binary phosphate glasses has been reported (Ref 15). Binary phosphate glasses containing sodium oxide (Na_2O), beryllium oxide (BeO), magnesium oxide (MgO), calcium oxide (CaO), strontium oxide (SrO), barium oxide (BaO), zinc oxide (ZnO), cadmium oxide (CdO), aluminum oxide (Al_2O_3), gallium oxide (Ga_2O_3), lead oxide (PbO), and bismuth oxide (Bi_2O_3) were used at metaphosphate stoichiometry. Several important vibrational bands were observed in the spectra. A band at 700 cm^{-1} was assigned to the symmetrical vibration of the –P–O–P– group. Bands observed from 1155 to 1230 cm^{-1} represent the symmetric and antisymmetric vibrations of the $-PO_2$ group.

Effects on the frequency and the intensity of these bands were observed upon addition of the above-mentioned cations to these glasses. A quadratic increase in frequency of the $-PO_2$ feature occurred with an increase in the ionic potential (charge-to-radius ratio) of the cation. However, a linear decrease in intensity of this band was observed with an increase

in ionic potential of the cation. These cationic dependencies were rationalized in terms of an increase in the ionic character of the oxygen-phosphorus bonds, P ··· O, as a result of the donor-acceptor interaction between oxygen and the metal, and oxygen and phosphorus.

Inclusions in glasses that contain gases associated with various chemical reactions and processing stages of glass formation have been studied (Ref 16). Because these inclusions generally degrade the appearance and mechanical strength of the glass, it is desirable to identify and eliminate their causes. Test samples were prepared for Raman analysis by bubbling carbon dioxide (CO_2) or sulfur dioxide (SO_2) through molten glass ($68SiO_2$-$14Na_2O$-$12BaO$-$6ZnO$). Raman bands associated with CO_2 and SO_2 were monitored, and their appearance correlated with the preparation conditions.

This approach was later expanded to the Raman analysis of glasses by using the Raman microprobe (MOLE) to characterize deposits and gaseous contents of bubbles in the glass (Ref 17). The MOLE technique enabled sampling of only the bubbles in the glass to the exclusion of the bulk glass matrix. In these studies, clear soda-lime-silica glass was prepared by the float glass process. Carbon dioxide and SO_2 gaseous inclusions were identified by their Raman bands at 1389 and 1286 cm^{-1} for CO_2 and 1151 cm^{-1} for SO_2. The ratio of the CO_2 to SO_2 concentrations was quantitatively determined by the relative band intensities to be 11:1. The Raman microprobe analysis further indicated that no nitrogen, oxygen, sulfite, or water vapor was present in the glass bubbles. However, solid deposits in the bubbles showed polymeric sulfur in the $S_\infty + S_8$ structure, as indicated by the Raman bands at 152, 216, and 470 cm^{-1}. Monitoring the 1151 cm^{-1} band of SO_2 revealed that the concentration of SO_2 in these bubbles can be decreased by heating to 450 °C (840 °F). The loss of SO_2 was attributed to the reaction:

$$2Na_2O + 3SO_2 \rightleftharpoons 2Na_2SO_4 + S$$

which also indicates the source of the sulfur deposits. Finally, the presence of sulfur or the absence of SO_2 in the bubbles was concluded to be a function of the cooling to which the glass is subjected during fabrication.

In a recent Raman characterization of SiO_2 glasses, the effect of alkali cations on the spectral response of SiO_2 glasses was monitored as a function of weight percent of lithium, sodium, potassium, rubidium, and cesium cations (Ref 18). High-frequency bands greater than 800 cm^{-1} have been assigned to the local distribution of silicon tetroxide (SiO_4) tetrahedra in these glasses. These features were found to be insensitive to large-scale clustering of alkali metal species. A Raman feature at 440 cm^{-1} is also characteristic of silica glass and indicates that regions of the three-dimensional SiO_4 network remain after introduction of the alkali metal cations. The intensity of the 440 cm^{-1} band was found to depend on the type of alkali metal cation introduced into the glass. This observation is thought to reflect a difference in the long-range distribution of the different cations. The conclusion was that the smaller cations, such as lithium, have a greater tendency to cluster than larger cations.

Another feature of the Raman characterization of glasses is that glasses have spectra that are usually similar to those of the corresponding molten electrolyte. This led to use of molten salts as models for glass systems. Molten salts can be condensed at temperatures well below T_g, the glass transition temperature, to form glassy salts.

Polymers

Polymers have traditionally been structurally analyzed using infrared vibrational techniques because of the lack of Raman sensitivity before development and widespread availability of laser excitation sources. Consequently, the identification schemes developed relied exclusively on the absence or presence of characteristic infrared active vibrational modes (Ref 19, 20). Nevertheless, because Raman analysis of polymer systems offers several advantages, many Raman investigations have appeared in the literature.

The weak Raman scattering of water makes the Raman analysis of polymers in aqueous media particularly attractive. Little sample preparation is required to obtain at least a survey spectrum of a polymer, and sample size and thickness present no problem as in infrared spectroscopy. One of the major advantages of Raman spectroscopy is the availability of the entire vibrational spectrum using one instrument. Vibrations that occur at frequencies lower than 50 cm^{-1} can be observed with little difficulty. The main problem that remains in handling polymeric samples involves sample fluorescence. The solution to this problem is similar to that used for other Raman samples and has been discussed above.

Infrared and Raman spectroscopy are complementary techniques. Neither can give all the information that a combination of the two techniques can provide because of differences in selection rules. However, depending on the type of information required, Raman spectroscopy can prove to be better suited for polymer characterization in terms of required sensitivity, simplicity of sampling methods, or vibrational region of interest.

One area of interest in the Raman characterization of polymers is the identification of components that may be present in only 5 to 10% concentrations. Studies of various types of degradation and polymerization have involved observing changes in vibrational features that affect only a small part of the polymer. In such cases, it is advantageous to monitor vibrational bands that are sensitive to the particular functional group that will reflect the change of interest. The dependence of Raman scattering intensity on changes in polarizability of a molecule makes it particularly sensitive to symmetrical vibrations and to vibrations involving larger atoms. In particular, Raman intensities are more sensitive than infrared for the detection of C=C, C≡C, phenyl, C–S, and S–S vibrations.

The structural identification of polymeric species is based on the presence or absence of characteristic vibrational modes. Many identification schemes are based exclusively on infrared active vibrational modes. Infrared bands at 1493, 1587, and 1605 cm^{-1} indicate the presence of phenyl functional groups. However, these are not particularly strong vibrations in the Raman spectrum. A useful feature of the Raman spectrum for polymers containing phenyl groups is the strong ring-breathing mode near 1000 cm^{-1}. In addition, the position of the band in this region indicates the type of ring substitution. A strong, sharp band near 1000 cm^{-1} is characteristic of mono-substituted, metadisubstituted, and 1,3,5-trisubstituted rings. Substitution in the ortho position can be differentiated from the above by the shift of this band to 1050 cm^{-1}. However, a band in this region is absent for para-substituted compounds. The presence of phenyl groups can also be characterized by a strong aromatic C–H stretch from 3000 to 3100 cm^{-1}.

The strong Raman vibration associated with the C=C symmetric stretch facilitates identification of trans-substituted alkene polymers and investigation of several polymerization reactions. In particular, Raman spectroscopic studies have been used to follow the polymerization of butadiene (Ref 21) and styrene (Ref 22). Raman results indicate that polymerization of butadiene proceeds by several competing mechanisms (Ref 21). Because the polymer products all contain an unsaturated skeletal backbone, the Raman active C=C stretching mode can be conveniently monitored during polymerization due to its enhanced sensitivity. In this study, the *trans*-1,4-butadiene product was identified by its Raman spectrum.

The thermal polymerization of styrene has also been investigated using Raman spectroscopy (Ref 22). The decrease in the intensity of the C=C stretch at 1632 cm^{-1}, relative to that of an internal standard, was used to obtain kinetic information on the styrene polymerization reaction. Values obtained for the activation energy and percent styrene conversion were found to be in reasonable agreement with results from other methods.

The intensity of the asymmetric C–H stretching vibration has been used to determine quantitatively the percent vinyl chloride in the vinyl chloride/vinylidene chloride copolymer (Ref 23). Calibration curves showed a linear relationship between the ratio of the intensity of the C–H stretch at 2906 cm^{-1} to the scattering reference up to 100% vinyl chloride with an accuracy of ±2%. By comparison, an analysis based on a characteristic infrared

absorption at 1205 cm^{-1} showed a correlation between vinyl chloride copolymer content and infrared intensity for concentrations only up to 25%.

Strong Raman vibrations of the S–S and C–S stretching modes in the regions from 400 to 500 cm^{-1} and 600 to 700 cm^{-1} are particularly useful for identification of polysulfides, because these modes are infrared inactive. These vibrational features have been used to investigate the structural changes accompanying vulcanization of *cis*-1,4-polybutadiene (Ref 24, 25). Several spectral features in these regions were assigned tentatively for vibrations corresponding to disulfide, polysulfide, and five- and six-membered thioalkane and thioalkene structures (Ref 24). The structures found after vulcanization varied with the length of time and temperature of the process (Ref 25). Corresponding information obtained from the C=C region provides information on skeletal chain modifications. The vibrational information from this spectral region suggests the formation of *cis*-1,4-*trans*-1,4, vinyl, and conjugated triene groups. The number of terminal mercapto groups in polythioethers has been quantitatively determined using the S–H stretching vibration at 2570 cm^{-1} (Ref 26). The method, based on a comparison of the peak area of the S–H band with that of an internal standard, has been shown to be effective to 0.5% mercapto group content with a precision of ±1%.

The Raman spectrum of aromatic silicones is characterized by a strong band near 500 cm^{-1} that is attributable to the symmetric Si–O–Si mode. The infrared-active asymmetric stretch is a strong, broad absorption from 1000 to 1100 cm^{-1} that overlaps characteristic bands due to vinyl and phenyl groups. Therefore, the determination of small amounts of vinyl and phenyl groups copolymerized in silicone systems is particularly well suited to Raman analysis. In addition, a Raman active C–Si stretch can be observed at 710 cm^{-1}. These Raman vibrational features have been used to investigate helix formation in polydimethylsiloxane (Ref 27). Depolarization measurements were obtained for the methyl C–H stretching mode at 2907 cm^{-1} and the Si–O–Si mode at 491 cm^{-1} as a function of temperature. Estimated values were obtained for the enthalpy of helix formation, the change in entropy, and the lower limit for the fraction of polymers existing in helix conformation.

A method has been devised to determine the percent conversion of polyacrylamide to poly (N-dimethylaminomethylacrylamide) using intensity ratios of the characteristic C=N stretching bands for the reactant at 1112 cm^{-1} and the product at 1212 cm^{-1} (Ref 28). The percent conversion results were in excellent agreement with results obtained using ^{13}C nuclear magnetic resonance (NMR).

Raman spectroscopic methods have been used to investigate formation of phenolformaldehyde resins (Ref 29). The polymerization reaction is carried out in aqueous media that severely limit applicability of infrared analysis. The intensity of four characteristic Raman bands were measured as a function of time during the early stages of the condensation reaction. Raman results were consistent with results obtained by the analysis of the reaction mixture using paper chromatography. However, the Raman results provide more detailed information on structural changes occurring during the early stages of the reaction.

The extent of crystallinity of polyethylene has been monitored using Raman spectroscopy (Ref 30). Crystallization of polyethylene was found to produce a marked narrowing of the Raman band corresponding to the C=O stretch at 1096 cm^{-1}. This change in bandwidth was correlated with density changes in the polymer and found to be a reliable indicator of the degree of crystallinity.

Graphites

Raman spectroscopy has been used extensively to characterize the extent of surface structural disorder in graphites. More recently, Raman spectroscopy has been developed to investigate intercalated graphites. The analysis of graphites is experimentally complicated by strong absorption of laser radiation, which has been observed to damage the surface significantly. To avoid significant surface decomposition during analysis, low laser powers (20 to 40 mW) on a stationary graphite sample are used. An alternate, more prevalent technique is the use of a rotating sample cell (Ref 14, 31, 32) with which higher incident powers (300 to 400 mW) can be used.

The utility of Raman spectroscopy for graphite characterization derives from the various vibrational behaviors observed for different graphites. Group theory predicts two Raman active modes for smooth single-crystalline graphite. These vibrations are an in-plane mode at 1581 cm^{-1} and a low-frequency plane rigid shear mode at 42 cm^{-1}. Single-crystalline and highly oriented pyrolytic graphite (HOPG) exhibits a single sharp vibrational feature near 1580 cm^{-1} (Ref 33). Less highly ordered graphites, such as activated charcoal, vitreous carbon, and stress-annealed pyrolytic graphite, show additional vibrational modes. A vibrational feature near 1355 cm^{-1} is associated with surface structural defects in the graphite lattice. The relative intensity of the 1355 cm^{-1} band to that of the 1580 cm^{-1} band increases with the degree of surface disorder (Ref 34). The behavior of the 1355 cm^{-1} feature has been used extensively to characterize the effects of annealing (Ref 35), grinding (Ref 36), mechanical polishing (Ref 37), and ion implantation (Ref 38, 39) on the structural integrity of various graphites.

A similar increase in the intensity of the 1355 cm^{-1} band occurs after electrochemical oxidation and reduction of HOPG in 0.05 *M* sulfuric acid (H_2SO_4) solution (Ref 31). An additional vibrational feature at 1620 cm^{-1} appears after oxidation at 800 °C (1470 °F) (Ref 37), mechanical polishing (Ref 37), and grinding (Ref 36) of various graphites. This feature has been associated with a hexagonal ring stretching mode that has been modified by formation of carbon-oxygen complexes near the graphite surface or crystallite edges (Ref 37).

Raman microprobe analysis has been used with transmission electron microscopy (TEM) to characterize vapor deposition of carbon films on alkali halide cleavages (Ref 40). These results indicate that the graphite films graphitize in five distinct stages characterized by the release of a given structural defect at each stage.

Raman spectroscopy has also been a valuable tool for the analysis of intercalated graphite species. These studies have focused on the vibrational behavior of donor intercalates, such as K^+ (Ref 41), Li^+ (Ref 42), Rb^+ (Ref 43), and Cs^+ (Ref 44), and acceptor intercalates, such as ferric chloride ($FeCl_3$) (Ref 45), bromine (Br_2) (Ref 46-48), iodine chloride (ICl) (Ref 48), and iodine bromide (IBr) (Ref 48) of various stage numbers. The stage number refers to the number of carbon layers between any pair of intercalant layers. Therefore, the number of carbon layers between intercalant layers increases with the stage number. Although there is general agreement of the Raman data for stage two and greater species, some controversy remains regarding stage one compounds (Ref 49).

Several models have been proposed to explain the Raman vibrational behavior observed for various intercalated species (Ref 44, 50, 51). The nearest layer model (Ref 44) is based on a perturbation of the pristine graphite modes by the presence of intercalate nearest neighbor layers. This model predicts that pure stage one and stage two donor or acceptor compounds should exhibit a single Raman band in the vicinity of but displaced from that of HOPG, near 1580 cm^{-1}. For stage three and higher compounds, an additional vibration near 1580 cm^{-1} is anticipated due to the presence of graphite layers that do not have intercalates as nearest neighbors. The intensity of the pristine graphite mode at 1580 cm^{-1} is expected to increase with the stage number relative to the displaced mode.

Several intercalate systems have been examined to test the nearest layer model. The Raman behavior of potassium (Ref 41) and rubidium (Ref 43) intercalated HOPG followed that predicted by the model. Further data analysis of the ratio of intensities of the 1581 cm^{-1} band to that of the displaced band as a function of stage number provides valuable information on charge transfer and charge localization in the various layers. The similarity in slope for potassium and rubidium cations indicates that both systems are electrically similar and that charge exchange to the carbon

layers is not completely localized (Ref 49). Qualitative spectral agreement has been observed for intercalated $FeCl_3$ (Ref 45), an acceptor intercalate.

Raman spectroscopy has also provided evidence for the intercalation of Br_2, ICl, and IBr as molecular entities (Ref 48). The high-frequency bands were found to be insensitive to the intercalant species. The position of the low-frequency band was found to depend on the nature of the intercalant. These low-frequency bands were assigned to intramolecular modes of the intercalant species. The strong wavelength dependence of the Br_2 intramolecular mode has been interpreted as a resonance-enhancement effect due to an electronic Br_2 excitation (Ref 46).

Analysis of Surfaces

Use of the laser as an intense monochromatic light source exploits the advantages of Raman spectroscopy in the vibrational analysis of surfaces and surface species while surmounting the inherent sensitivity limitations of the technique that would preclude its applicability to surfaces. Moreover, Raman spectroscopy adequately overcomes several limitations of infrared spectroscopy, which has been used extensively over the past several decades to provide vibrational information on surfaces and surface species.

An advantage of Raman spectroscopy is its ready accessibility to the low-frequency region of the spectrum. Vibrational behavior can be characterized as close to the Rayleigh line as 10 cm^{-1} with conventional instrumentation. This frequency region, particularly below 200 cm^{-1}, is not accessible with infrared detectors. Such low-frequency data are important in the complete vibrational analysis of surface species, especially for investigations of the nature of the chemical interaction of a surface species with the underlying surface.

Raman spectroscopy is also valuable in probing surface processes in aqueous environments due to the extreme weakness of the Raman scattering of water. This advantage has made feasible the vibrational characterization of such materials problems in aqueous environments as corrosion. A third problem with infrared analysis of certain surface systems that Raman overcomes is interference from absorption of the radiation by the underlying bulk material. In particular, this advantage has been realized in the study of metal oxide systems. These species are strong infrared absorbers, but only weak to moderate Raman scatters.

Surface Structure of Materials

The study of metal oxide and supported metal oxide catalysts best illustrates application of Raman spectroscopy to analysis of the surface structure of materials. An example of the Raman analysis of metal oxide surface structure is a study on the effect of specific chemical treatments on the surface structure of molybdenum oxide catalysts used for coal hydrosulfurization (Ref 52). Raman surface spectra characteristic of molybdenum disulfide (MoS_2) after sulfidation of the catalyst by H_2/H_2S were observed. After these catalysts were used for coal hydrosulfurization, the Raman spectra were dominated by intense scattering characteristic of carbon. Furthermore, the Raman analysis of used catalysts subjected to regeneration showed that all the original features of the unused catalysts are not recovered in regeneration (Ref 52).

Raman spectroscopy has been used extensively to characterize the surface structure of supported metal oxides. The Raman investigation of chemical species formed during the calcination and activation of tungsten trioxide (WO_3) catalysts supported on silica (SiO_2) and alumina (Al_2O_3) has been documented (Ref 53). These Raman results indicate that crystalline and polymeric forms of WO_3 are present on SiO_2-supported surfaces. However, only polymeric forms of WO_3 are present on γ-Al_2O_3 supports.

Vanadium oxide catalysts supported on γ-Al_2O_3, cerium dioxide (CeO_2), chromium oxide (Cr_2O_3), SiO_2, titanium dioxide (TiO_2), and zirconium dioxide (ZrO_2) have been characterized using Raman spectroscopy (Ref 54). These catalysts are of industrial importance for the oxidation Of SO_2, CO, and other hydrocarbons. In this study, the effects of catalyst preparation and catalyst surface coverage on the Raman vibrational behavior were investigated. For low surface coverages of vanadium oxide (1 to 40 wt%) on any support, the Raman spectra were found to be characteristic of a two-dimensional surface vanadate phase. This behavior was found to be independent of catalyst preparation. For medium to high surface coverages of vanadium oxide on any support, the wet-impregnated preparation method resulted in a crystalline V_2O_5 surface phase.

Many Raman characterization studies have been performed on the effects of the nature of the support, the presence of other metals, impregnation order, molybdenum oxide loading, pH, and calcination and regeneration conditions on the resulting surface structure of molybdena catalysts (Ref 55-61). Results indicate the presence of MoO_3 or MoO_4^{2-} surface species. An example of these studies is the Raman investigation of molybdena catalyst supported on γ-Al_2O_3 and n-Al_2O_3 (Ref 61). Various catalysts were prepared by impregnation from aqueous molybdate solutions of pH 6 and 11, and the development of the final catalytic moiety was followed using Raman spectroscopy and ultraviolet photoelectron spectroscopy (UPS). Vibrational modes of surface species were assigned on the basis of solution spectra of various isopolymolybdates. Results show that the initial species undergoes ion exchange with surface hydroxides to form MoO_4^{2-} regardless of the solution pH, and depending on the surface coverage of MoO_4^{2-}, the formation of Mo–O–Mo bridging species can occur during subsequent preparation to give a final polymeric surface species.

Surface Species on Nonmetals

One of the most prevalent chemical probes of the surface chemical environment in adsorption studies is pyridine. Its utility as a surface probe stems from the extreme sensitivity of the ring-breathing vibrational modes to chemical environment. Furthermore, its π-electron system, which is responsible for the large Raman scattering cross section for this molecule, makes pyridine useful for Raman studies in terms of detectability. Assignments of the ring-breathing vibrational modes of adsorbed pyridine species are usually made by comparison to a series of model environments of the pyridine molecule. Table 1 lists the accepted model environments for pyridine. The various interactions produce substantial shifts in the peak frequency, ν_1, of the symmetrical ring-breathing vibration of pyridine. In general, the more strongly interacting the lone pair of electrons on the pyridine nitrogen, the larger the shift in ν_1 to higher frequencies.

Similar behavior in the ν_1, ring-breathing mode of pyridine is observed when pyridine adsorbs to various metal oxide and related solid surfaces. Table 2 summarizes the Raman studies performed on pyridine adsorbed on diverse adsorbents. In general, for high coverages of pyridine on any solid adsorbent, the Raman spectrum closely resembles that of liquid pyridine. In these cases, the interaction of the pyridine with the underlying adsorbent is thought to be weak. Therefore, the pyridine is considered physisorbed.

Two types of strong interaction of pyridine with the underlying adsorbent are possible for low coverages of pyridine on metal oxide and related surfaces. Hydrogen-bonded pyridinium surface species can be formed at Brönsted sites on the surface. These species give rise to the ν_1 pyridine band near 1010 cm^{-1}. Strong chemisorption of the pyridine species can also occur at Lewis acid sites, such as Al^{3+}, on these surfaces. This type of interaction produces the higher frequency ν_1 band near 1020 cm^{-1}.

In the Raman spectroscopy of pyridine on X and Y zeolites, the frequency of the ν_1 symmetric ring-breathing mode can be linearly correlated with the electrostatic potential (charge-to-radius ratio) of the balancing cation within the cation-exchange zeolite (Ref 13, 67, 69, 70). This correlation has been interpreted as indicating pyridinecation interactions of varying strength in these systems. The strength of interaction of pyridine with the cation is thought to increase with the electrostatic potential of the cation, as indicated by the corresponding shift of ν_1 to higher frequencies.

Table 1 Model environments for pyridine vibrational behavior

Model compound	ν_1/cm	Nature of interaction	Ref
Pyr	991	Neat liquid	62
Pyr in $CHCl_3$	998	H-bond	12, 13, 63
Pyr in CH_2Cl_2	992	No interaction	12, 13, 63
Pyr in CCl_4	991	No interaction	12, 13, 63
Pyr in H_2O	1003	H-bond	12, 13, 63–65
$PyrH^+$ BF_4^-	1012	Pyridinium	64, 65
Pyr:$ZnCl_2$	1025	Coordinately bound	12, 64, 65
Pyr N-Oxide	1016	Coordinately bound	63
Pyr:$GaCl_3$ (benzene solution)	1021	Coordinately bound	12

Table 2 Vibrational behavior of adsorbed pyridine

Adsorption environment	ν_1/cm	Nature of interaction	Ref
Pyr	991	Neat liquid	62
Pyr/chromatographic grade silica	1010	Lewis acid site	12, 13, 63
Pyr/Cab-O-Sil HS5 (high coverage)	991	Physisorption	63
Pyr/Cab-O-Sil HS5 (low coverage)	1010	H-bonded	63
Pyr/aerosil	1006	H-bonded	63
Pyr/silica with excess Al^{3+}	1020	Lewis acid site	63
Pyr/porous vycor glass	1006	H-bonded	11
Pyr/γ-Al_2O_3	1019	Lewis acid site	13, 63, 66
Pyr/*n*-Al_2O_3	1019	Lewis acid site	63
Pyr/chlorided γ-Al_2O_3	1022	Lewis acid site	67, 68
Pyr/chlorided *n*-Al_2O_3	1022	Lewis acid site	63
Pyr/13% Al_2O_3-silica(a)	1007, 1020	Lewis acid site and H-bonded	66, 68
Pyr/13% Al_2O_3-silica(b)	999	Physisorption	66, 68
Pyr/TiO_2	1016	Lewis acid site	63
Pyr/NH_4^+ -mordenite	1004	H-bonded	63
Pyr/magnesium oxide	991	Physisorption	63
Pyr/zeolites (X and Y)	998–1020	Physisorption and Lewis acid site	13, 69, 70

(a) Low temperature pretreament. (b) High temperature pretreatment

Another feature of the pyridine surface studies that has important implications is the linear increase in pyridine band intensity with coverage (Ref 71). This observation suggests the utility of Raman spectroscopy as a probe of adsorption isotherms for surface species. Such studies may be significant in understanding catalytic systems that are important in industry.

Raman microprobe characterization of pyridine adsorbed on metal oxide surfaces has been reported. Pyridine adsorbed on Ni-Mo-γ-Al_2O_3 has been studied using the Raman microprobe (MOLE) (Ref 72). The catalyst used was 3 wt% nickel oxide (NiO) and 14 wt% molybdenum trioxide (MoO_3) with γ-Al_2O_3. The ν_1 feature of pyridine at 1014 cm^{-1} was attributed to pyridine chemisorbed at Lewis acid sites. It was determined that the physisorbed pyridine can be removed by heating to 100 °C (212 °F) as monitored by the disappearance of the bands at 991 and 1031 cm^{-1}. The chemisorbed pyridine remained on the surface even after heating to 200 °C (390 °F). The similarity between these results and those for pyridine on Co-Mo-γ-Al_2O_3 (Ref 73) was noted.

Corrosion on Metals

Raman spectroscopy is finding widespread use in the characterization of corrosion processes on metal surfaces. Corrosion can be easily monitored under gas phase or liquid conditions. The principal advantage of using Raman spectroscopy for corrosion is in corrosive aqueous environments, such as acidic or alkaline solutions, in which the Raman scattering of the aqueous medium is weak and does not interfere with detection of the metal corrosion products. Most of the corrosion products of interest involve metal oxide species. Due to the relatively weak scattering of metal oxides, Raman spectroscopy was not successfully applied to the *in situ* characterization of corrosion until the use of lasers as excitation sources had become commonplace. However, advances in this materials characterization area since the late 1970s suggest that the Raman investigation of corrosive environments has the potential to provide much molecularly specific information about metal surface corrosion products, such as chemical composition, stoichiometry, and crystallographic phase.

In situ Raman spectroscopy has been used to study the surface oxides formed on common alloys during oxidation at elevated temperatures in air (Ref 74). By comparison of the surface spectra with those of mixed pure oxides, metal oxides, such as ferric oxide (Fe_2O_3), chromic oxide (Cr_2O_3), nickel oxide (NiO), and manganese chromite ($MnCr_2O_4$), were identified.

In a more recent gas-phase corrosion study, the chemical composition of iron oxide films formed on iron by air oxidation at 400 °C (750 °F) for 2 h were identified using Raman spectroscopy (Ref 75). The characteristic lattice vibrations of the different iron oxides enabled differentiation between Fe_2O_3 and iron oxide (Fe_3O_4) films. Further analysis using Ar^+ sputtering and Raman spectroscopy to depth-profile the oxide layer formed revealed the presence of two zones of different oxides. Raman spectra obtained after various sputtering times indicated that the composition of this two-zone layer was 200 nm Fe_2O_3 on 800 nm Fe_3O_4.

Electrochemically based corrosion systems in aqueous environments have been studied using Raman spectroscopy. The Raman characterization of the galvanostatic reduction of different crystallographic forms of FeOOH on weathering steel surfaces has been reported (Ref 76). Atmospheric corrosion of metals has been explained relative to the electrochemical response of the metal in which different regions of the metal act as anode and cathode of the electrochemical cell. This study was motivated by a previous claim that an inner layer of α-FeOOH is formed on weathering steels under atmospheric corrosion conditions. This layer of α-FeOOH presumably resists electrochemical reduction to Fe_3O_4 such that, upon formation of a layer of α-FeOOH of sufficient thickness, further corrosion is inhibited. The results of this study confirmed the previous claims. The Raman intensity of the 300 and 380 cm^{-1} bands of α-FeOOH were monitored in an electrochemical cell under reducing conditions. No change in intensity of these bands was observed, suggesting that no significant reduction of α-FeOOH occurs after 9 h.

Similar studies indicated that Fe_3 also is not reduced after 9 h under these conditions. In contrast, γ-FeOOH is reduced to Fe_3O_4, as shown by the disappearance of the band at 258 cm^{-1} and the appearance of the Fe_3O_4 band at 675 cm^{-1}. Furthermore, amorphous FeOOH can also be reduced to Fe_3O_4. Amorphous FeOOH is reduced more easily than γ-FeOOH. The overall conclusions of this study were that three of the four polymorphs of FeOOH present on weathering steels can be reduced to Fe_3O_4. The only form of FeOOH that resists reduction is γ-FeOOH.

Several reports of the Raman characterization of the corrosion of lead surfaces have appeared in the literature. Early research on lead in 0.1 *M* sulfate solutions showed the presence of surface films of compositions not in complete agreement with the predictions of the Pourbaix (potential-pH) diagram (Ref 77). The Pourbaix diagram does not predict the formation of lead oxide (PbO) under any conditions. However, the recorded spectra indicated the presence of PbO at certain potentials in acid and neutral solutions and at all potentials above the immunity region in basic solutions. Despite the lack of agreement of the Raman spectra with the Pourbaix diagrams, the Raman spectra were in agreement with the potentiodynamic polarization curves for these systems.

A later study of this system helped to resolve the above-mentioned anomalies (Ref 78). The objective of this study was to monitor the surface phases formed on lead during potentiodynamic cycling to obtain information on the cycle life and failure mechanisms in lead-acid batteries. The approach used was to anodize lead foils and acquire Raman spectra of the resulting lead surface films formed under potential control and after removal from the electrochemical cell. The surface spectra were then compared with spectra of the corresponding pure lead oxide for assignment. Lead surfaces anodized at −0.45 V versus a mercury/mercurous sulfate (Hg/Hg_2SO_4) reference electrode for 12 to 72 h were covered by a film of lead sulfate ($PbSO_4$), as indicated by bands at 436, 450, and 980 cm^{-1}. The surface expected to exist for lead anodized at +1.34 V versus Hg/Hg_2SO_4 is β-PbO_2, according to the Pourbaix diagram. This surface phase for *in situ* or *ex situ* analysis cannot be assigned unequivocally to this oxide in agreement with the previous study. Evidence for damage of the original phase due to laser irradiation was noted, however. Bands were observed that suggested that the β-PbO_2 film is converted to PbO during irradiation.

Raman spectroscopy has been used to study the oxidation of silver electrodes in alkaline environments (Ref 79). Earlier studies on this system suggested a two-step oxidation process of silver in which silver oxide (Ag_2O) is formed followed by further oxidation to AgO. It was also known that Ag_2O could be photoelectrochemically oxidized to AgO. However, the mechanism of this process was controversial. Therefore, this study was undertaken to monitor this process *in situ*.

Ex situ Raman analysis of silver electrodes anodized at +0.6 V versus a mercury/mercuric oxide (Hg/HgO) reference electrode showed no distinct vibrational features, although the Pourbaix diagram for this system predicts the formation of Ag_2O. Therefore, the Ag_2O was concluded to be a weak Raman scatterer or decomposed in the laser beam. However, *ex situ* Raman analysis of silver electrodes anodized at +0.8 V showed a strong peak at 430 cm^{-1}, with weaker features at 221 and 480 cm^{-1}. The surface phase formed at this potential was assigned to AgO by comparison with the Raman spectrum obtained on a sample of pure AgO.

When these analyses were performed *in situ* under potential control, the spectrum of AgO was always observed regardless of the applied potential. This observation was explained as evidence for the photoelectrochemical conversion of Ag_2O to AgO. The kinetics of this conversion were followed with Raman spectroscopy in potential step experiments in which the growth of the 430 cm^{-1} AgO band was monitored as a function of time.

Raman spectroscopy has been used to characterize the corrosion of nickel and cobalt in aqueous alkaline media (Ref 80). The metals were anodized in 0.05 *M* sodium hydroxide (NaOH), and the Raman spectra of the surface phases were acquired. Comparison of the surface phase formed on nickel with various pure oxides of nickel indicated the presence of $Ni_2O_{3.4}\cdot 2H_2O$, with vibrational bands at 477 and 555 cm^{-1}. The surface phase formed during anodization of cobalt was determined to be a mixture of cobaltous oxide (CoO), with Raman bands a 515 and 690 cm^{-1}, and cobalt oxide (Co_3O_4), with bands at 475 and 587 cm^{-1}. These assignments were also confirmed by comparison of the surface spectra with those of the pure cobalt oxides.

Surface-Enhanced Raman Scattering

The sensitivity constraints imposed by the normal Raman-scattering effect severely limits applicability of this technique to the study of species on smooth and low-surface-area area surfaces. Therefore, Raman characterization of monolayer amounts of materials on metals was not feasible for some time. A significant advance in this field that prompted surface Raman spectroscopy was the 1973 Raman study of mercurous chloride (Hg_2Cl_2), mercurous bromide (Hg_2Br_2), and mercuric oxide (HgO) on a thin mercury film electrode in an operating electrochemical environment (Ref 81). Pyridine adsorbed at silver and copper electrodes was also studied (Ref 82, 83). Spectra of good quality were presented and attributed to a monolayer of adsorbed pyridine on high-surface-area silver and copper electrodes produced by anodization.

In 1977, it was recognized that the pyridine/silver spectra were anomalously intense (Ref 84, 85). The intensity enhancement of the pyridine surface species was estimated at approximately 10^5 to $10^6\times$ that which would be expected for an equivalent amount of pyridine in solution. This began the extensive investigation of the phenomenon known appropriately as surface-enhanced Raman scattering (SERS). Since the early efforts in this field, a variety of adsorbates at metal surfaces have been studied. An extensive list has been compiled of atomic and molecular species whose surface vibrational behavior has been characterized using SERS (Ref 86). An in-depth review of the field through 1981 has also been published (Ref 87).

In addition, SERS can be observed in diverse materials environments. Along with the metal/solution studies performed as indicated above, SERS investigations have been readily performed at metal/gas and metal/vacuum interfaces (Ref 87-90) as well as metal/solid interfaces in tunnel junction structures (Ref 87, 91, 92).

The major limitation of SERS as a materials characterization tool is that surface enhancement is not supported by all surfaces. Only a limited number of metals can support surface enhancement. The list of metals for which SERS has been documented remains controversial. Although the three most prevalent SERS metals are silver, copper, and gold (Ref 87), other metals have also been previously demonstrated or claimed to exhibit SERS.

The alkali metals lithium and potassium exhibit SERS in a vacuum environment for adsorbed benzene (Ref 93). Several reports of surface enhancement at platinum in a vacuum, sol (a suspension of metal colloids), and electrochemical environments have appeared (Ref 94-96). A brief report of the SERS of pyridine adsorbed at a cadmium electrode appeared in 1981 (Ref 97). Palladium (Ref 98) and nickel (Ref 99, 100) have been claimed to support SERS in vacuum environments. Beta-PdH electrodes are capable of surface enhancement of adsorbed pyridine and CO (Ref 101). Several recent reports of surface enhancement on semiconductor surfaces have also appeared. The SERS spectra of pyridine on NiO and TiO_2 surfaces in the gas phase have been reported (Ref 102, 103).

The general use of SERS as a surface characterization tool involves serious limitations. However, the potential for chemical modification of nonenhancing surfaces to allow for surface enhancement is under investigation. Surface-enhanced Raman scattering from pyridine adsorbed at a platinum electrode modified by small amounts of electrochemically deposited silver has been reported (Ref 104).

A similar approach has been used to investigate species adsorbed onto GaAs semiconductor surfaces (Ref 105, 106). Surface-enhanced resonant Raman scattering from $Ru(bipyridine)_3^{2+}$ has been observed on *n*-GaAs modified with small islands of electrochemically deposited silver (Ref 105). Normal SERS from $Ru(bipyridine)_3^{2+}$ has been documented on a silver-modified *p*-GaAs[100] electrode (Ref 106), and SERS has been reported from molecules adsorbed on thin gold overlayers on silver island films (Ref 107). These studies suggest that the potential exists in many systems for suitable modification of the surface to exploit the increase in sensitivity provided by SERS.

Relative to the restrictions imposed by the limited metals that can support SERS, it is necessary to determine the surface properties required for surface enhancement (Ref 87, 108). Proposed theoretical contributions to SERS can be classified as electromagnetic and chemical. The surface properties required to activate the chemical contributions fully are subtle and have eluded systematic investigation. The requisite surface properties necessary for electromagnetic effects are better understood and have begun to yield to systematic investigation. The latter include surface roughness and surface dielectric properties. These properties are related, because surface roughness dictates the resulting surface electronic structure.

Electromagnetic enhancement effects are based on the enhanced electric field found at roughness features on metal surfaces having

the appropriate dielectric properties. The role of surface roughness has been recognized in electrochemical SERS (Ref 84). However, the anodization procedure used in these systems has not been completely investigated. Research is underway to understand systematically the chemistry, electrochemistry, and resulting surface morphology of the electrochemically generated surface roughness in SERS (Ref 109).

Systematic studies of the functional relationship between the extent of surface enhancement and surface dielectric properties are in their infancy. One approach in electrochemical systems is to alter the surface dielectric properties of an electrode by electrochemically depositing submonolayer and monolayer amounts of a foreign, that is, different metal (Ref 104, 110-113). The ability of that surface to support SERS for an adsorbate can then be correlated with some parameter describing electronic properties of the surface (Ref 113). This approach may yield a level of predictability about whether or not the surface of a new material can support SERS.

Despite the lack of general applicability of SERS, the wealth of information this technique can yield warrants further study. The ease of acquiring Raman spectral data from surface-enhancing systems is unsurpassed due to the remarkable intensities observed. Therefore, SERS should continue to receive consideration as a tool capable of providing molecular vibrational information about surfaces and interfaces. Although SERS will probably never gain acceptance as a general surface analytical tool, it can and should be used with other vibrational surface probes, such as infrared spectroscopy, to help provide a complete molecular picture of a given surface or interface.

Exploration of SERS for the study of relevant materials systems has only begun. Surface-enhanced Raman scattering has been used to study catalytic oxidation of nitric oxide (NO), nitrogen dioxide (NO_2), nitrogen peroxide (N_2O_4), and sulfur dioxide (SO_2) on silver powders. Surface SO_3^{2-} was detected on the surface of silver powder exposed to SO_2 gas in a helium atmosphere. Further, thermal desorption as SO_2 and oxidation to SO_4^{2-} were followed spectroscopically as the temperature was slowly raised to 108 °C (225 °F) in an oxygen-containing atmosphere (Ref 114). In a later study, brief exposure of oxygenated silver powder to NO and NO_2/N_2O_4 gases was found to result in SERS spectra of NO_2^- and NO_3^- (Ref 115).

The electropolymerization of phenol on silver electrodes in the presence and absence of amines has been studied using SERS (Ref 116). Results show the polymerization to be similar to that observed on iron. Surface-enhanced Raman scattering elucidation of the role of amines in polymerization indicates that amines displace phenoxide ions, which are adsorbed flat at the silver surface, and allow formation of thick protective films of the polymer (Ref 116). Further SERS studies on this system involving the role of the surfactant Triton in improving the adhesion characteristics of the polymer on the silver substrate have revealed that Triton is found at the silver/polymer interface and is dispersed throughout the polymer, chemically bonding to the polymer after curing in air (Ref 117).

The interest in SERS has signified the desirability of vibrational information about species at metal surfaces. This has led to the development of the technology for performing surface Raman measurements on metals without enhancement. The availability of sensitive multichannel detectors and appropriate optical components compatible with such systems has enabled obtainment of surface Raman spectra of molecules adsorbed on smooth metal surfaces. The first successful demonstration of surface Raman spectroscopy without enhancement was published in 1982 (Ref 118). High-quality Raman spectra from molecules adsorbed on well-characterized surfaces at low coverage were reported. The unenhanced Raman approach has since been used for the Raman spectroscopic investigation of molecules in tunnel junction structures (Ref 119) and metal/gas environments (Ref 120-122).

REFERENCES

1. C.V. Raman and K.S. Krishnan , *Nature*, Vol 122, 1928, p 501
2. D.A. Long, *Raman Spectroscopy*, McGraw-Hill, 1977
3. M.C. Tobin, *Laser Raman Spectroscopy*, John Wiley & Sons, 1971
4. D.C. O'Shea, W.R. Callen, and W.T. Rhodes, *Introduction to Lasers and Their Applications*, Addison-Wesley, 1977
5. Spex Industries, Metuchen, NJ, 1981
6. E.E. Wahlstrom, *Optical Crystallography*, 4th ed., John Wiley & Sons, 1969
7. M. Delhaye and P. Dhemalincourt, *J. Raman Spectrosc.*, Vol 3, 1975, p 33
8. P. Dhamelincourt, F. Wallart, M. Leclercq, A.T. NGuyen, and D.O. Landon, *Anal. Chem.*, Vol 51, 1979, p 414A
9. P.J. Hendra and E.J. Loader, *Trans. Faraday Soc.*, Vol 67, 1971, p 828
10. E. Buechler and J. Turkevich, *J. Phys. Chem.*, Vol 76, 1977, p 2325
11. T.A. Egerton, A. Hardin, Y. Kozirovski, and N. Sheppard, *Chem. Commun.*, 1971, p 887
12. R.O. Kagel, *J. Phys. Chem.*, Vol 74, 1970, p 4518
13. T.A. Egerton, A.H. Hardin, Y. Kozirovski, and N. Sheppard, *J. Catal.*, Vol 32, 1974, p 343
14. W. Kiefer and H.J. Bernstein, *Appl. Spectrosc.*, Vol 25, 1971, p 609
15. Y.S. Bobovich, *Opt. Spectrosc.*, Vol 13, 1962, p 274
16. G.J. Rosasco and J.H. Simmons, *Am. Cer. Soc. Bull.*, Vol 53, 1974, p 626
17. G.J. Rosasco and J.H. Simmons, *Am. Cer. Soc. Bull.*, Vol 54, 1975, p 590
18. D.W. Matson and S.K. Sharma, *J. Noncryst. Solids*, Vol 58, 1983, p 323
19. H.J. Sloane, in *Polymer Characterization: Interdisciplinary Approaches*, C. Craver, Ed., Plenum Press, 1971, p 15–36
20. R.E. Kagarise and L.A. Weinberger, "Infrared Spectra of Plastics and Resins," Report 4369, Naval Research Laboratory, Washington, DC, 26 May 1954
21. J.L. Koenig, *Chem. Technol.*, 1972, p 411
22. B. Chu and G. Fytas, *Macromolecules*, Vol 14, 1981, p 395
23. J.L. Koenig and M. Meeks, *J. Polymer Sci.*, Vol 9, 1971, p 717
24. J.L. Koenig, M.M. Coleman, J.R. Shelton, and P.H. Stramer, *Rubber Chem. Technol.*, Vol 44, 1971, p 71
25. J.R. Shelton, J.L. Koenig and M.M. Coleman, *Rubber Chem. Technol.*, Vol 44, 1971, p 904
26. S. K. Mukherjee, G.D. Guenther, and A. K. Battacharya, *Anal. Chem.*, Vol 50, 1978, p 1591
27. A.J. Hartley and I.W. Sheppard, *J. Polymer Sci.*, Vol 14, 1976, p 64B
28. B.R. Loy, R.W. Chrisman, R.A. Nyquist, and C.L. Putzig, *Appl. Spectrosc.*, Vol 33, 1979, p 174
29. S. Chow and Y.L. Chow, *J. Appl. Polymer Sci.*, Vol 18, 1974, p 735
30. A.J. Melveger, *J. Polymer Sci.*, A2, Vol 10, 1972, p 317
31. A.J. McQuillan and R.E. Hester, *J. Raman Spectrosc.*, Vol 15, 1984, p 17
32. T.P. Mernagh, R.P. Cooney, and R.A. Johnson, *Carbon*, Vol 22, 1984, p 1
33. F. Tunistra and J. L. Koenig, *J. Chem. Phys.*, Vol 53, 1970, p 1126
34. M. Nakamizo, R. Kammerzck, and P.L. Walker, *Carbon*, Vol 12, 1974, p 259
35. M. Nakamizo, *Carbon*, Vol 15, 1977, p 295
36. M. Nakamizo, *Carbon*, Vol 16, 1978, p 281
37. M. Nakamizo and K. Tami, *Carbon*, Vol 22, 1984, p 197
38. B.S. Elman, M.S. Dresselhaus, G. Dresselhaus, E.W. Maby, and H. Mazurek, *Phys. Rev. B.*, Vol 24, 1981, p 1027
39. B.S. Elman, M. Shayegan, M.S. Dresselhaus, H. Mazurek, and G. Dresselhaus, *Phys. Rev. B.*, Vol 25, 1982, p 4142
40. J.M. Rouzand, A. Oberlin, and C. Beny-Bassez, *Thin Solid Films*, Vol 105, 1983, p 75
41. N. Caswell and S.A. Solin, *Bull. Am. Phys. Soc.*, Vol 23, 1978, p 218
42. P.C. Eklund, G. Dresselhaus, M.S. Dresselhaus, and J.E. Fischer, *Phys. Rev. B.*, Vol 21, 1980, p 4705
43. S.A. Solin, *Mater. Sci. Eng.*, Vol 31, 1977, p 153
44. R.J. Nemanich, S.A. Solin, and D. Guerard, *Phys. Rev. B.*, Vol 16, 1977, p 2965

45. N. Caswell and S.A. Solin, *Solid State Commun*., Vol 27, 1978, p 961
46. P.C. Eklund, N. Kambe, G. Dresselhaus, and M.S. Dresselhaus, *Phys. Rev. B*., Vol 18, 1978, p 7068
47. A. Erbil, G. Dresselhaus, and M.S. Dresselhaus, *Phys. Rev. B*., Vol 25, 1982, p 5451
48. J.J. Song, D.D.L. Chung, P.C. Eklund, and M.S. Dresselhaus, *Solid State Commun*., Vol 20, 1976, p 1111
49. S.A. Solin, *Physica B & C*, Vol 99, 1980, p 443
50. S.Y. Leng, M.S. Dresselhaus, and G. Dresselhaus, *Physica B & C*, Vol 105, 1981, p 375
51. H. Miyazaki, T. Hatana, T. Kusunaki, T. Watanabe, and C. Horie, *Physica B & C*, Vol 105, 1981, p 381
52. J. Medema, C. van Stam, V.H.J. deBear, A.J.A. Konings, and D.C. Konigsberger, *J. Catal*., Vol 53, 1978, p 385
53. R. Thomas, J.A. Moulijn, and F.R.J. Kerkof, *Recl. Trav. Chim. Pays-Bas*., Vol 96, 1977, p m134
54. F. Roozeboom and M.C. Metelmeijer-Hazeleger, *J. Phys. Chem*., Vol 84, 1980, p 2783
55. B.A. Morrow, Vibrational Spectroscopies for Adsorbed Species, in *ACS Symposium Series No. 137*, A.T. Bell and M.L. Hair, Ed., American Chemical Society, Washington, 1980
56. F.R. Brown, L.E. Makovsky, and K.H. Ree, *J. Catal*., Vol 50, 1977, p 385
57. C.P. Cheng and G.L. Schrader, *J. Catal*., Vol 60, 1979, p 276
58. H. Knozinger and H. Jeziorowski, *J. Phys. Chem*., Vol 82, 1978, p 2002
59. D.S. Znigg, L.E. Makovsky, R.E. Tischer, F.R. Brown, and D.M. Hercules, *J. Phys. Chem*., Vol 84, 1980, p 2898
60. F.R. Brown, L.E. Makovsky, and K.H. Rhee, *J. Catal*., Vol 50, 1977, p 162
61. H. Jeziorowski and H. Knozinger, *J. Phys. Chem*., Vol 83, 1979, p 1166
62. J.K. Wilhurst and H.J. Bemstein, *Can. J. Chem*., Vol 35, 1957, p 1183
63. P.J. Hendra, J.R. Horder, and E.J. Loader, *J. Chem. Soc. A*, 1971, p 1766
64. R.P. Cooney and T.T. Nguyen, *Aust. J. Chem*., Vol 29, 1976, p 507
65. R.P. Cooney, T.T. Nguyen, and G.C. Curthoys, *Adv. Catal*., Vol 24, 1975, p 293
66. P.J. Hendra, I.D.M. Turner, E.J. Loader, and M. Stacey, *J. Phys. Chem*., Vol 78, 1974, p 300
67. T.A. Egerton and A.H. Hardin, *Catal. Rev. Sci. Eng*., Vol 11, 1975, p 1
68. P.J. Hendra, A.J. McQuillan, and I.D.M. Turner, *Dechema*, Vol 78, 1975, p 271
69. T.A. Egerton, A.H. Hardin, and N. Sheppard, *Can. J. Chem*., Vol 54, 1976, p 586
70. A.H. Hardin, M. Klemes, and B.A. Morrow, *J. Catal*., Vol 62, 1980, p 316
71. R.P. Cooney and N.T. Tam, *Aust. J. Chem*., Vol 29, 1976, p 507
72. E. Payen, M.C. Dhamelincourt, P. Dhamelincourt, J. Grimblot, and J.P. Bonnelle, *Appl. Spectrosc*., Vol 36, 1982, p 30
73. C.P. Cheng, and G.L. Schrader, *Spectrosc. Lett*., Vol 12, 1979, p 857
74. R.L. Farrow, R.E. Benner, A.S. Nagelberg, and P.L. Mattern, *Thin Solid Films*, Vol 73, 1980, p 353
75. J.C. Hamilton, B.E. Mills, and R.E. Benner, *Appl. Phys. Lett*., Vol 40, 1982, p 499
76. J.T. Keiser, C.W. Brown, and R.H. Heidersbach, *J. Electrochem. Soc*., Vol 129, 1982, p 2686
77. R. Thibeau, C.W. Brown, G. Goldfarb, and R.H. Heidersbach, *J. Electrochem. Soc*., Vol 127, 1980, p 37
78. R. Varma, C.A. Melendres, and N.P. Yao, *J. Electrochem. Soc*., Vol 127, 1980, p 1416
79. R. Kötz and E. Yeager, *J Electroanal. Chem*., Vol 111, 1980, p 105
80. C. A. Melendres and S. Xu, *J. Electrochem. Soc*., Vol 131, 1984, p 2239
81. M. Fleischmann, P.J. Hendra, and A.J. McQuillan, *J. Chem. Soc. Chem. Comm*., Vol 3, 1973, p 80
82. M. Fleischmann, P.J. Hendra, and A.J. McQuillan, *Chem. Phys. Lett*., Vol 26, 1974, p 163
83. R.L. Paul, A.J. McQuillan, P.J. Hendra, and M. Fleischmann, *J. Electroanal. Chem*., Vol 66, 1975, p 248
84. D.L. Jeanmaire and R.P. VanDuyne, *J. Electroanal. Chem*., Vol 84, 1977, p 1
85. M.G. Albrecht and J.A. Creighton, *J. Am. Chem. Soc*., Vol 99, 1977, p 5215
86. H. Seki, *J. Electron Spectrosc, Related Phenom*., Vol 30, 1983, p 287
87. R.K. Chang and T.E. Furtak, Ed., *Surface Enhanced Raman Scattering*, Plenum Press, 1982
88. T.H. Wood and M.V. Klein, *J. Vac. Sci. Technol*., Vol 16, 1979, p 459
89. J.E. Rowe, C.V. Shank, D.A. Zwemet, and C.A. Murray, *Phys. Rev. Lett*., Vol 44, 1980, p 1770
90. H. Seki and M.R. Philpott, *J. Chem. Phys*., Vol 73, 1980, p 5376
91. J.C. Tsang and J.R. Kirtley, Light Scattering in Solids, in *Proceedings of Second Joint USA-USSR Symposium*, J.L. Birman, H.Z. Cummins, and K.K. Rebane, Ed., Plenum Press, 1979, p 499
92. J.C. Tsang and J.R. Kirtley, *Solid State Commun*., Vol 30, 1979, p 617
93. M. Moskovits and D.P. DiLella, in *Surface Enhanced Raman Scattering*, R.K. Chang and T.E. Furtak, Ed., Plenum Press, 1982, p 243
94. H. Yamada, Y. Yamamoto, and N. Tani, *Chem. Phys. Lett*., Vol 86, 1982, p 397
95. R.E. Benner, K.U. van Raben, K.C. Lee, J.F. Owen, R.K. Chang, and B.L. Laube, *Chem. Phys. Lett*., Vol 96, 1983, p 65
96. B.H. Loo, *J. Phys. Chem*., Vol 87, 1983, p 3003
97. B.H. Loo, *J. Chem. Phys*., Vol 75, 1981, p 5955
98. B.H. Loo, *J. Electron Spectrosc. Related Phenom*., Vol 29, 1983, p 407
99. C.C. Chou, C.E. Reed, J.C. Hemminger, and S. Ushioda, *J. Electron Spectrosc. Related Phenom*., Vol 29, 1983, p 401
100. H. Yamada, N. Tani, and Y. Yamamoto, *J. Electron Spectrosc. Related Phenom*., Vol 30, 1983, p 13
101. M. Fleischmann, P.R. Graves, J.R. Hill, and J. Robinson, *Chem. Phys. Lett*., Vol 95, 1983, p 322
102. H. Yamada, N. Tani, and Y. Yamamoto, *J. Electron Spectrosc. Related Phenom*., Vol 30, 1983, p 13
103. H. Yamada and Y. Yamamoto, *Surf. Sci*., Vol 134, 1983, p 71
104. J. E. Pemberton, *J. Electroanal. Chem*., Vol 167, 1984, p 317
105. R.P. Van Duyne and J.P. Haushalter, *J. Phys. Chem*., Vol 87, 1983, p 2999
106. Y. Mo, H. van Känel, and P. Wachter, *Solid State Commun*., Vol 52, 1984, p 213
107. C.A. Murray, *J. Electron Spectrosc. Related Phenom*., Vol 29, 1983, p 371
108. G.C. Schatz, *Acc. Chem. Res*., Vol 17, 1984, p 370
109. D.D. Tuschel, J.E. Pemberton, and J.E. Cook, *Langmuir*, Vol 2, 1986
110. B. Pettinger and L. Moerl, *J. Electron Spectrosc. Related Phenom*., Vol 29, 1983, p 383
111. L. Moerl and B. Pettinger, *Solid State Commun*., Vol 43, 1982, p 315
112. T. Watanabe, N. Yanigaraha, K. Honda, B. Pettinger, and L. Moerl, *Chem. Phys. Lett*., Vol 96, 1983, p 649
113. A.L. Guy, B. Bergami, and J.E. Pemberton, *Surf. Sci*., Vol 150, 1985, p 226
114. P.B. Dorain, K.U. Von Raben, R.K. Chang, and B.L. Laube, *Chem. Phys. Lett*., Vol 84, 1981, p 405
115. K.U. Von Raben, P.B. Dorain, T.T. Chen, and R.K. Chang, *Chem. Phys. Lett*., Vol 95, 1983, p 269
116. M. Fleischmann, I.R. Hill, G. Mengoli, and M.M. Musiani, *Electrochim. Acta*, Vol 28, 1983, p 1545
117. G. Mengoli, M.M. Musiani, B. Pelli, M. Fleischmann, and I.R. Hill, *Electrochim. Acta*, Vol 28, 1983, p 1733
118. A. Campion, J.K. Brown, and V.M. Grizzle, *Surf Sci*., Vol 115, 1982, p L153
119. J.C. Tsang, Ph. Avouris, and J.R. Kirtley, *Chem. Phys. Lett*., Vol 94, 1983, p 172
120. A. Campion and D.R. Mullins, *Chem. Phys. Lett*., Vol 94, 1983, p 576
121. V.M. Hallmark and A. Campion, *Chem. Phys. Lett*., Vol 110, 1984, p 561
122. D. R. Mullins and A. Campion, *Chem. Phys. Lett*., Vol 110, 1984, p 565